Ultracold collisions in the presence of synthetic spin-orbit coupling

Hao Duan, Li You, and Bo Gao

Phys. Rev. A **87**, 052708 — Published 20 May 2013

DOI: 10.1103/PhysRevA.87.052708

Ultracold collision in the presence of synthetic spin-orbit coupling

Hao Duan,[1] Li You,[1,*] and Bo Gao[2,†]

[1] *State Key Laboratory of Low-Dimensional Quantum Physics, Department of Physics, Tsinghua University, Beijing 100084, China*

[2] *Department of Physics and Astronomy, Mailstop 111, University of Toledo, Toledo, Ohio 43606, USA*

(Dated: May 6, 2013)

We present an analytical description for ultracold collisions between two spin-$\frac{1}{2}$ fermions with isotropic spin-orbit coupling (SOC) of the Rashba type. We show that regardless of how weak the SOC may be, at sufficiently low energies the collision properties are significantly modified. The ubiquitous low energy Wigner threshold behavior is changed and its modified form for ground state neutral atoms is given. The particles are further found to scatter preferentially into the lower-energy helicity states due to the breaking of parity conservation. This latter point establishes interaction with SOC as one mechanism for the spontaneous emergence of handedness. Our theory is applicable both to elementary spin-$\frac{1}{2}$ fermions such as electrons in condensed matter and to ultracold pseudo spin-$\frac{1}{2}$ atoms such as ^{6}Li in its ground hyperfine state.

PACS numbers: 34.50.Cx,67.85.Lm,71.70.Ej,05.30.Fk

I. INTRODUCTION

Systems of cold atoms have become fertile laboratories for many-body and few-body physics largely because of the ability to tune and manipulate atomic interactions. The magnetic Feshbach resonance [1], for instance, has allowed precise tuning of scattering length to virtually arbitrary value, facilitating studies of strongly coupled many-body systems [2] and also few-body systems in the universal regime [3–5].

A new class of manipulation of cold atoms has arisen recently under the general envelope of synthetic gauge fields, generated mainly through coherent laser-atom interactions [6]. Among various types, the synthetic spin-orbit coupling (SOC) [7–10] is of special interest as it simulates a type of coupling that is regarded as important in fractional quantum Hall effect and topological insulators [11, 12]. SOC naturally arises in relativistic quantum theory. For electrons in graphene, a thorough theoretical treatment of the elastic scattering theory for two-dimensional Dirac fermions was presented in Ref. [13]. This study will focus on ultracold atoms, between which the scattering is always 3 dimensional (3D) and non-relativistic, even when confined in reduced dimensions. Despite a large body of recent works on SOC systems [9, 14–23], many fundamental questions remain to be answered, as elementary as effects of SOC on the two-body scattering in 3D [24–26].

Among the active recent studies of atomic quantum gases in the presence of synthetic gauge fields, most take the simple approximation keeping the bare form of contact pseudo potentials between two atoms in the absence of SOC intact, while treating synthetic gauge potential terms as additional single atom interactions. A recent experiment by Williams *et al.* [27] provides an early indication that such an approach can be problematic. The presence of SOC could give rise to substantial and essential modifications for understanding interacting many-body and few-body systems at low energies. It is therefore of significant interest to find out how gauge potential interaction terms will modify atomic low energy scattering. In particular, one wishes to find out if keeping the same contact pseudo potential as if SOC were absent remains true or not. While a perturbative argument in favor of adopting the same contact pseudo potential is widely assumed, one is confronted by a self-consistency issue: if the various scattering amplitudes will change or not.

This work presents a general theoretical treatment for the scattering of two spin-$\frac{1}{2}$ fermions in the presence of isotropic Rashba type SOC. We provide explicit forms of the self-consistent scattering amplitudes that low energy pseudo potential needs to satisfy when SOC is present. As we report in this article, despite being a single particle interaction, the Rashba type SOC modifies the dispersion relations and the thresholds for the asymptotic states, which consequently change significantly the low energy scattering amplitude as well as other scattering properties between two atoms. We demonstrate this result by studying collisions of two spin-1/2 fermions under SOC. We pick spin-$\frac{1}{2}$ fermions for its relevance to electrons in condensed matter, and for the fact that it can be simulated with ^{6}Li in its ground hyperfine state [10] and other two state subsystems of fermionic atom isotopes such as ^{40}K [8, 9]. We choose isotropic coupling to isolate the effects of SOC and effects of anisotropy. Additionally, the simple isotropic coupling allows for analytical solutions which greatly facilitate the digestion as well as the discovery of the new results reported here. Based on the coupled channel method we develop and the modified Wigner threshold behavior we report, we expect multichannel numerical calculations for the anisotropic SOC such as the experimentally realized single term SOC $\propto \sigma_x p_x$ [7] can be carried out analogously to the low energy scattering

* lyou@mail.tsinghua.edu.cn

† bo.gao@utoledo.edu

between two fixed direction atomic dipoles [28].

The isotropic Rashba SOC we discuss is a non-Abelian type gauge field that persists to infinite separation. As we discuss in this study, it substantially changes the scattering formulation, including the very definitions of fundamental quantities such as the incoming and outgoing states and their associated scattering matrices. The formalism we develop for the scattering including SOC is outlined below in detail in sections II and III, and is solved analytically in terms of scattering in the absence of SOC, by taking advantage of a length scale separation [29, 30]. The results and discussions are given in section IV. When compared with the results in the absence of SOC, we find a substantially altered threshold behavior, different from the familiar Wigner behavior [31], and a preferential scattering into the lower-energy helicity state as a consequence of parity non-conservation. This preference implies that handedness can spontaneously emerge as a result of scattering with SOC. While the full implications of our results on many-body physics with ultracold atoms are to be explored elsewhere, it is clear that they will open interesting possibilities for understanding and control of atomic quantum gases with SOC. Our results are summarized in the conclusion section.

II. OUR MODEL

This section starts with the introduction of the model system we consider: the scattering between two atoms with isotropic Rashba type SOC. We also take this opportunity to conveniently introduce several relevant scattering properties when SOC is absent. A single spin-1/2 atom in the presence of the isotropic Rashba type SOC is then reviewed, with the modified dispersion relations, thresholds for scattering states, and the helicity states given out in explicit detail. Finally, we discuss atomic flux density for the single atom eigenstates in the presence of a gauge field such as SOC. The canonical and kinetic momentum are in general different with a gauge field, which is crucial point for obtaining the correct scattering amplitudes and cross sections.

We consider two identical particles with $F_1 = F_2 = 1/2$. We use symbols F_1 and F_2 to emphasize that for composite particles such as atoms, the "spin" refers to the total angular momentum of an individual particle. In the absence of SOC, the interaction between such two particles can very generally be described by the Hamiltonian

$$H = \mathcal{H}_1 + \mathcal{H}_2 + \widehat{V}, \tag{1}$$

where $\mathcal{H}_i = \boldsymbol{p}_i^2/2m$ is the single particle Hamiltonian in the absence of SOC, and $\widehat{V}$ is an interaction operator describing two effective central potentials: $V^{(F=0)}(r)$ for the singlet states and $V^{(F=1)}(r)$ for the triplet states. Without SOC, the total "spin", $\boldsymbol{F} = \boldsymbol{F}_1 + \boldsymbol{F}_2$, and the relative orbital angular momentum between the two particles $\boldsymbol{l}$ are independently conserved. The scattering is thus fully characterized by two effective single-channel K matrices with elements, $\tan\delta_l^{F=0}$ for the "singlet" states and $\tan\delta_l^{F=1}$ for the "triplet" states [32]. For ultracold atoms, these two sets of phase shifts are equivalently characterized at zero energy by the respective scattering lengths for the two potentials. More generally they can be described using either the multichannel quantum-defect theory (MQDT) [29], or the QDT expansion [33, 34].

The isotropic SOC of the Rashba type changes the single particle Hamiltonian from $\mathcal{H} = \boldsymbol{p}^2/2m$ to

$$\mathcal{H} = \frac{\boldsymbol{p}^2}{2m} + \frac{\hbar}{m} C_{\rm so} \boldsymbol{\sigma}\cdot\boldsymbol{p}, \tag{2}$$

where $\boldsymbol{\sigma}$ denotes the Pauli spin matrix, $C_{\rm so}$ is a constant characterizing the strength of SOC. It has the dimension of a k-vector (inverse length), with its magnitude to be denoted by $k_{\rm so} \equiv |C_{\rm so}|$. The corresponding energy scale for SOC is $s_E = \hbar^2 k_{\rm so}^2/m$. This above single particle Hamiltonian (2) is diagonalized by states $|\pm, \boldsymbol{n}_{\rm so}\rangle|\boldsymbol{k}\rangle$, where $|\boldsymbol{k}\rangle$ describes the translational motion, and is an eigenstate of $\boldsymbol{p}$ with an eigenvalue of $\hbar\boldsymbol{k}$. $|\pm, \boldsymbol{n}_{\rm so}\rangle$ is a short-hand notation for $|F = 1/2, M = \pm 1/2, \boldsymbol{n}_{\rm so}\rangle$ with $\boldsymbol{n}_{\rm so}$ defining the direction of quantization. More explicitly, in position and z-axis quantized spinor representation, they take the form

$$\begin{aligned}\psi_+(\boldsymbol{r},\chi) &= \langle \boldsymbol{r},\chi|+,\boldsymbol{n}_{\rm so}\rangle|\boldsymbol{k}\rangle \\ &= \frac{1}{(2\pi)^{3/2}} e^{i\boldsymbol{k}\cdot\boldsymbol{r}} \begin{pmatrix} \cos(\theta_{\rm so}/2) \\ \sin(\theta_{\rm so}/2) e^{i\phi_{\rm so}} \end{pmatrix}, \end{aligned} \tag{3}$$

$$\begin{aligned}\psi_-(\boldsymbol{r},\chi) &= \langle \boldsymbol{r},\chi|-,\boldsymbol{n}_{\rm so}\rangle|\boldsymbol{k}\rangle \\ &= \frac{1}{(2\pi)^{3/2}} e^{i\boldsymbol{k}\cdot\boldsymbol{r}} \begin{pmatrix} \sin(\theta_{\rm so}/2) \\ -\cos(\theta_{\rm so}/2) e^{i\phi_{\rm so}} \end{pmatrix}, \end{aligned} \tag{4}$$

where $(\theta_{\rm so}, \phi_{\rm so})$ are the angles specifying the direction vector $\boldsymbol{n}_{\rm so}$. In the above two eigenstates (3) and (4) for the single particle Hamiltonian (2), $e^{i\boldsymbol{k}\cdot\boldsymbol{r}}$ is the corresponding plane wave, and the two component spinors are the internal spin wave functions expressed along the lab fixed z-quantization axis. We will generally call them the helicity states.

For the isotropic Rashba type SOC, $\boldsymbol{n}_{\rm so} = \hat{\boldsymbol{k}} = \boldsymbol{k}/k$, when $C_{\rm so} > 0$. One can simply switch to $\boldsymbol{n}_{\rm so} = -\hat{\boldsymbol{k}} = -\boldsymbol{k}/k$ for $C_{\rm so} < 0$, with all results remaining intact. For the same k, the "$\pm$" states have different energies as given by the distinctively different dispersion relations: $E_\pm = \hbar^2k^2/2m \pm \hbar^2 k_{\rm so} k/m$. For a fixed energy E, the "$\pm$" states corresponds to different canonical momentum $k_\pm = \sqrt{k^2 + k_{\rm so}^2} \pm k_{\rm so}$ satisfying the dispersion relations: $E = \hbar^2 k_\pm^2/2m \pm \hbar^2 k_{\rm so} k_\pm/m$ as shown in Fig. 1. In order to simplify notation, we assume in the following, $C_{\rm so} > 0$. This corresponds to taking $\boldsymbol{n}_{\rm so} = \hat{\boldsymbol{k}}$, or the direction of the canonical momentum $\boldsymbol{k}$ for a single particle in free space.

The scattering cross sections are properly defined in terms of the ratios of the scattered particle flux densities to the incoming flux density [35]. At the single particle

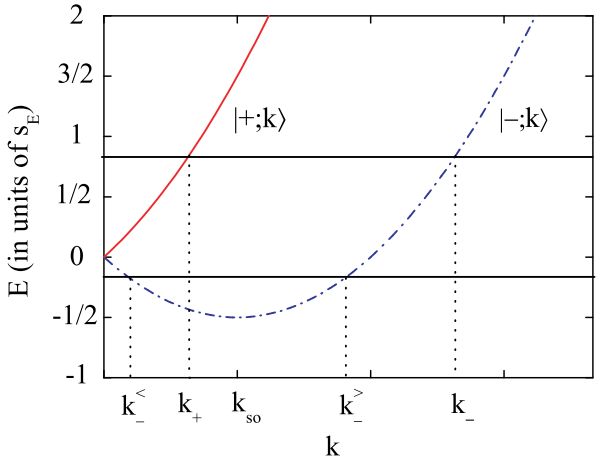

FIG. 1. (Color online) The dispersion curve for the helicity state $|\pm, \boldsymbol{n}_{\rm so}\rangle|\boldsymbol{k}\rangle$ of a single pseudo spin-$\frac{1}{2}$ atom with isotropic Rashba SOC. The two branches correspond respectively to the higher energy ("+") and lower energy ("−") states when $C_{\rm so} > 0$. At each energy $E = \hbar^2k^2/2m > 0$, the "±" states correspond to different k_+ and k_-. When $E < 0$, the two intersection points are labeled by $k_-^<$ and $k_-^>$ respectively. Both belong to the same lower energy helicity branch. $s_E = \hbar^2k_{\rm so}^2/2\mu$ is the energy scale for the SOC.

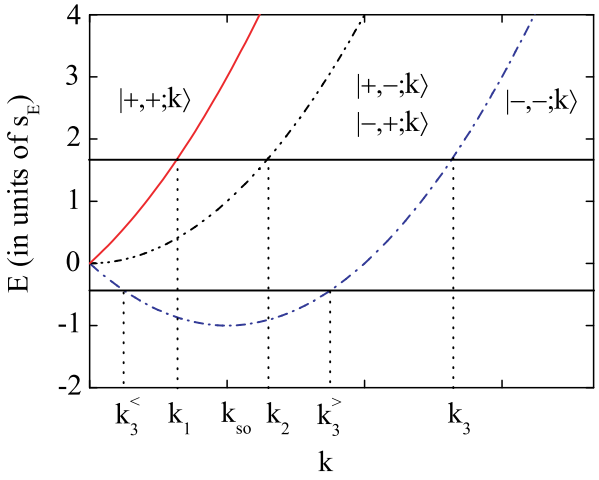

FIG. 2. (color online) The three branches of dispersion for two particles with SOC in the center-of-mass frame. For each energy $E = \hbar^2k^2/2\mu > 0$, the three corresponding k's, given in the order of increasing magnitude, are $k_1 = \sqrt{k_{\rm so}^2 + k^2} - k_{\rm so}$ for the $|+,+;\boldsymbol{k}_1\rangle$ state, $k_2 = k$ for the $|+,-;\boldsymbol{k}_2\rangle$ and $|-,+;\boldsymbol{k}_2\rangle$ states, and $k_3 = \sqrt{k_{\rm so}^2 + k^2} + k_{\rm so}$ for the $|-,-;\boldsymbol{k}_3\rangle$ state. As in Fig. 1 for a single atom, for $E < 0$ the two intersection points are labeled by $k_3^<$ and $k_3^>$ respectively, belong to the same lowest energy branch.

level, the effect of SOC on particle flux is already clearly visible. Thus, we need to revisit in detail the probability flux, $\boldsymbol{j}(\boldsymbol{r})$, which is the diagonal element of a probability flux *operator* in the coordinate representation, traced over the spin degrees of freedom. More specifically, we find

$$\boldsymbol{j}(\boldsymbol{r}) = {\rm Tr}_{\rm spin}\langle\boldsymbol{r}|\widehat{\boldsymbol{j}}|\boldsymbol{r}\rangle \ , \tag{5}$$

where $\widehat{\boldsymbol{j}}$ is the flux operator, defined in a pure state $|\psi\rangle$ by

$$\widehat{\boldsymbol{j}} = \frac{1}{2}\left[\,\widehat{\boldsymbol{v}}|\psi\rangle\langle\psi| + |\psi\rangle\langle\psi|\widehat{\boldsymbol{v}}\,\right] \ , \tag{6}$$

in which $\widehat{\boldsymbol{v}}$ is the velocity operator defined by $\widehat{\boldsymbol{v}} = \dot{\widehat{\boldsymbol{r}}} = [\widehat{\boldsymbol{r}}, \mathcal{H}]/i\hbar$. In the absence of SOC, $\widehat{\boldsymbol{v}} = \widehat{\boldsymbol{p}}/m$, and the flux reduces to its standard form [35]. With SOC, the velocity operator becomes $\widehat{\boldsymbol{v}} = \widehat{\boldsymbol{p}}/m + \hbar C_{\rm so}\boldsymbol{\sigma}/m$. For the two helicity states (3) and (4), we find the flux densities

$$\boldsymbol{j}(\boldsymbol{r}) = \frac{\hbar}{m}\sqrt{k_{\rm so}^2 + k^2}\ \hat{\boldsymbol{k}}_\pm, \tag{7}$$

for $E > 0$ with $k = \sqrt{2mE/\hbar^2}$. When $-\hbar^2k_{\rm so}^2/2m < E < 0$, we find

$$\boldsymbol{j}_-^<(\boldsymbol{r}) = -\frac{\hbar}{m}\sqrt{k_{\rm so}^2 - \kappa^2}\ \hat{\boldsymbol{k}}_-^<, \tag{8}$$

$$\boldsymbol{j}_-^>(\boldsymbol{r}) = \frac{\hbar}{m}\sqrt{k_{\rm so}^2 - \kappa^2}\ \hat{\boldsymbol{k}}_-^>, \tag{9}$$

with $\kappa = \sqrt{-2mE/\hbar^2}$. In the latter case of $E < 0$, the "+" helicity channel is closed while there now exist two "−" helicity states with $k_-^< = k_{\rm so} - \sqrt{k_{\rm so}^2 - \kappa^2}$ and $k_-^> = k_{\rm so} + \sqrt{k_{\rm so}^2 - \kappa^2}$.

For scattering at $E > 0$, the case that we consider in this paper, the important single-particle property in SOC is the one as implied by Eq. (7). At a fixed energy, the "±" states have different phase velocity, given by $\boldsymbol{p}/(2m) \to \hbar\boldsymbol{k}_\pm/(2m)$, but the same group velocity and/or flux density, given by Eq. (7).

III. SCATTERING BETWEEN TWO ATOMS

This section presents our detailed development of a proper framework for studying collisions in the presence of the single particle SOC. In atomic physics, SOC often refers to an interaction of the form $\propto \boldsymbol{\sigma}\cdot\boldsymbol{l}$, where $\boldsymbol{l}$ is the orbital angular momentum. For instance, the atomic fine structure interaction is of this form and can be understood in terms of the interaction of atomic spin with its own magnetic field due to orbital motion. Theoretical treatment for collision in the presence of $\boldsymbol{\sigma}\cdot\boldsymbol{l}$ type SOC are standard textbook material and can be found in [35, 36].

The SOC under investigation here is more precisely a spin-momentum coupling $\propto \boldsymbol{\sigma}\cdot\boldsymbol{p}$, which is often encountered in condensed matter physics. Unlike $\boldsymbol{\sigma}\cdot\boldsymbol{l}$, parity conservation is violated by the Rashba type SOC interaction $\boldsymbol{\sigma}\cdot\boldsymbol{p}$. To investigate the scattering properties between two particles under SOC, we need to proceed with extra care, properly identify all relevant steps in a scattering calculation: from the classification of the scatter-

ing channels, the identification of the incoming and the outgoing scattering states, to the proper construction of the scattering matrices. We will carry out the above steps in this section, formulating a suitable theory for treating scattering in the presence of SOC. To our knowledge, we are not aware of any framework of scattering theory directly adaptable to the SOC $\propto \boldsymbol{\sigma}\cdot\boldsymbol{p}$ considered in this study.

For two atoms in the presence of the isotropic Rashba type SOC and interacting through a central potential $\widehat{V}$, as described by Eq. (1), the conservation of their total canonical momentum, $\boldsymbol{P}=\boldsymbol{p}_1+\boldsymbol{p}_2$, allows the investigation of scattering in the center-of-mass frame, $\boldsymbol{P}=0$. The relative motion is described by the Hamiltonian

$$H_{\rm rel}=\frac{\boldsymbol{p}^2}{2\mu}+\widehat{V}+\frac{\hbar}{m}C_{\rm so}(\boldsymbol{\sigma}_1-\boldsymbol{\sigma}_2)\cdot\boldsymbol{p}, \tag{10}$$

where $\mu=m/2$ is the reduced mass, and $\boldsymbol{p}$ is the (canonical) momentum for the relative motion. In this center-of-mass frame, making use of the helicity states (3) and (4) introduced above for a single spin-$\frac{1}{2}$ atom in the presence of SOC, we find that at large inter-particle separation when $\widehat{V}$ is negligible, the single dispersion relation, $E=\hbar^2k^2/2\mu$, applicable to all spin states without SOC, changes into three branches: $E=(\hbar^2/2\mu)(k_1^2+2k_{\rm so}k_1)$ for the two-particle spin state $|+,\hat{\boldsymbol{k}}_1\rangle_1|+,-\hat{\boldsymbol{k}}_1\rangle_2$, $E=\hbar^2k_2^2/2\mu$ for the $|+,\hat{\boldsymbol{k}}_2\rangle_1|-,-\hat{\boldsymbol{k}}_2\rangle_2$ and $|-,\hat{\boldsymbol{k}}_2\rangle_1|+,-\hat{\boldsymbol{k}}_2\rangle_2$ spin states, and $E=(\hbar^2/2\mu)(k_3^2-2k_{\rm so}k_3)$ for the $|-,\hat{\boldsymbol{k}}_3\rangle_1|-,-\hat{\boldsymbol{k}}_3\rangle_2$ spin state. The helicity state ket indices 1 and 2 denote atoms 1 and 2 respectively. This change of dispersion is one of the key characteristics for two-atom collision in the presence of single atom SOC. The three branches of dispersion curves are illustrated in Fig. 2.

The four spin states for two atoms introduced above constitute what we call the two-particle helicity states. The different dispersion relations for the $|+,\hat{\boldsymbol{k}}_1\rangle_1|+,-\hat{\boldsymbol{k}}_1\rangle_2$ and $|-,\hat{\boldsymbol{k}}_3\rangle_1|-,-\hat{\boldsymbol{k}}_3\rangle_2$ states, which are related to each other by a parity operation, are direct consequences of the parity non-conservation nature of the Rashba type SOC we consider. The time-reversal symmetry is, however, still maintained. The two states $|+,\hat{\boldsymbol{k}}_2\rangle_1|-,-\hat{\boldsymbol{k}}_2\rangle_2$ and $|-,\hat{\boldsymbol{k}}_2\rangle_1|+,-\hat{\boldsymbol{k}}_2\rangle_2$ are also related to each other through a parity operation.

For two identical fermions in the asymptotic region when the interatomic potential is negligible, the antisymmetric states at the same energy of E can be easily constructed to be

$$\begin{aligned}
&|+,+;\boldsymbol{k}_1\rangle_{\rm in}\\
&=\frac{1}{\sqrt{2}}(|+,\hat{\boldsymbol{k}}_1\rangle_1|+,-\hat{\boldsymbol{k}}_1\rangle_2|\boldsymbol{k}_1\rangle-|+,-\hat{\boldsymbol{k}}_1\rangle_1|+,\hat{\boldsymbol{k}}_1\rangle_2|-\boldsymbol{k}_1\rangle),\\
&|+,-;\boldsymbol{k}_2\rangle_{\rm in}=\frac{1}{\sqrt{2}}|+,\hat{\boldsymbol{k}}_2\rangle_1|-,-\hat{\boldsymbol{k}}_2\rangle_2(|\boldsymbol{k}_2\rangle-|-\boldsymbol{k}_2\rangle),\\
&|-,+;\boldsymbol{k}_2\rangle_{\rm in}=\frac{1}{\sqrt{2}}|-,\hat{\boldsymbol{k}}_2\rangle_1|+,-\hat{\boldsymbol{k}}_2\rangle_2(|\boldsymbol{k}_2\rangle-|-\boldsymbol{k}_2\rangle),\\
&|-,-;\boldsymbol{k}_3\rangle_{\rm in}\\
&=\frac{1}{\sqrt{2}}(|-,\hat{\boldsymbol{k}}_3\rangle_1|-,-\hat{\boldsymbol{k}}_3\rangle_2|\boldsymbol{k}_3\rangle-|-,\hat{\boldsymbol{k}}_3\rangle_1|-,-\hat{\boldsymbol{k}}_3\rangle_2|-\boldsymbol{k}_3\rangle),
\end{aligned} \tag{11}$$

where $|\boldsymbol{k}_j\rangle$ denotes the nominal plane wave function with momentum $\boldsymbol{k}_j$. When no ambiguity arises, we will adopt a shorthand notation to index the incoming states, using $|1\rangle_{\rm in}$ for $|+,+;\boldsymbol{k}_1\rangle_{\rm in}$ and $|3\rangle_{\rm in}$ for $|-,-;\boldsymbol{k}_3\rangle_{\rm in}$ to index the various matrix elements within the lowest total angular momentum subspace of $F_t=0$.

As in Eqs. (3) and (4) for a single atom, we can express the above states in the position and lab fixed z-quantization axis spinor representation. For example, we find

$$\begin{aligned}
\Phi_1(\boldsymbol{r},\chi_1,\chi_2)&=\langle\boldsymbol{r},\chi_1,\chi_2|+,+;\boldsymbol{k}_1\rangle\\
&=\frac{i}{2\sqrt{2}}\left[e^{i\boldsymbol{k}_1\cdot\boldsymbol{r}}\begin{pmatrix}-e^{-i\phi_{k_1}}\sin\theta_{k_1}\\1+\cos\theta_{k_1}\\-1+\cos\theta_{k_1}\\e^{i\phi_{k_1}}\sin\theta_{k_1}\end{pmatrix}\right.\\
&\qquad\left.-e^{-i\boldsymbol{k}_1\cdot\boldsymbol{r}}\begin{pmatrix}-e^{-i\phi_{k_1}}\sin\theta_{k_1}\\-1+\cos\theta_{k_1}\\1+\cos\theta_{k_1}\\e^{i\phi_{k_1}}\sin\theta_{k_1}\end{pmatrix}\right],
\end{aligned} \tag{12}$$

where χ_1 and χ_2 are now spinors for atom 1 and 2 respectively, and the four row spinor represents the two-atom internal spin state in their joint z-quantization representation. From top to down respectively corresponding to their direct product spin states $|+,\hat{\boldsymbol{z}}\rangle_1|+,\hat{\boldsymbol{z}}\rangle_2$, $|+,\hat{\boldsymbol{z}}\rangle_1|-,\hat{\boldsymbol{z}}\rangle_2$, $|-,\hat{\boldsymbol{z}}\rangle_1|+,\hat{\boldsymbol{z}}\rangle_2$, $|-,\hat{\boldsymbol{z}}\rangle_1|-,\hat{\boldsymbol{z}}\rangle_2$. Similarly, one can find the explicit forms for

$$\begin{aligned}
\Phi_2(\boldsymbol{r},\chi_1,\chi_2)&=\langle\boldsymbol{r},\chi_1,\chi_2|+,-;\boldsymbol{k}_2\rangle,\\
\Phi_3(\boldsymbol{r},\chi_1,\chi_2)&=\langle\boldsymbol{r},\chi_1,\chi_2|-,+;\boldsymbol{k}_2\rangle,\\
\Phi_4(\boldsymbol{r},\chi_1,\chi_2)&=\langle\boldsymbol{r},\chi_1,\chi_2|-,-;\boldsymbol{k}_3\rangle.
\end{aligned} \tag{13}$$

Each of the above four states constitutes a proper "incoming" state, analogous to the incoming plane wave $\propto e^{ikz}$ (taken to be along the z-axis drection) for single channel scattering of a spinless particle. This study concerns the scattering between two identical fermions, therefore antisymmetrization is enforced on the total wave functions. The particle flux density for each of the relative motion incoming state (11) can be easily computed analogous to the single particle results of (7) and (8) or (9). We find in the asymptotically large r region

and for scattering at $E > 0$, the flux densities are respectively given by: $\hbar\sqrt{k_{\rm so}^2 + k^2}/\mu$ for states $|+,+;\boldsymbol{k}_1\rangle_{\rm in}$ and $|-,-;\boldsymbol{k}_3\rangle_{\rm in}$, and $\hbar k/\mu$ for states $|+,-;\boldsymbol{k}_2\rangle_{\rm in}$ and $|-,+;\boldsymbol{k}_2\rangle_{\rm in}$. Compared with the single atom results in the previous section, the particle mass is now replaced by the reduced mass $\mu = m/2$.

We now describe the structure of collision channels. In the presence of SOC, even the isotropic Rashba SOC under consideration here, $\boldsymbol{F}$ and $\boldsymbol{l}$ are generally no longer independently conserved. However, the total angular momentum $\boldsymbol{F}_t = \boldsymbol{F} + \boldsymbol{l}$ is conserved. The wave function for each total angular momentum, $F_t M_t$, can be expanded as follows

$$\psi_\eta^{F_t M_t} = \sum_\alpha \Theta_\alpha^{F_t M_t} G_{\alpha\eta}^{F_t}(r)/r \ ,$$

where $G_\alpha^{F_t}/r$ describes the relative radial motion, and η is an index for different linearly independent solutions. The $\Theta_\alpha^{F_t M_t}$ are channel functions, indexed by α, describing all degrees of freedom other than the relative radial motion. They are conveniently chosen here to be the $\{F, l\}$ basis, in which the interaction in the absence of SOC is diagonal. The summation over α, namely the $\{F, l\}$ combinations, is restricted both by the angular momentum conservation and by $F + l =$ even as imposed by the symmetry under the exchange of particles [37]. This leads to the following general channel structure for interaction with isotropic SOC. All $F_t =$ odd states are described by single-channel problems with the triplet potential $V^{(F=1)}(r)$, corresponding to $\{F = 1, l = F_t\}$. All $F_t =$ even states, other than $F_t = 0$, are described by three-channel problems, corresponding to $\{F = 0, l = F_t\}$, $\{F = 1, l = F_t - 1\}$, and $\{F = 1, l = F_t + 1\}$. The $F_t = 0$ states are described by a two-channel problem with $\{F = 0, l = 0\}$ and $\{F = 1, l = 1\}$.

The SOC term $\hbar(\boldsymbol{\sigma}_1 - \boldsymbol{\sigma}_2)\cdot\boldsymbol{p}/m$ in the two-atom scattering Hamiltonian (10) commutes with total angular momentum $\boldsymbol{F}_t$. Thus, one can find their common eigenstates. In each of the above discussed subspace labeled by $\{F, l\}$, the scattered wave function for each $F_t M_t$ can be expanded in terms of the following four outgoing internal states with their helicities defined with respect to the $\hat{\boldsymbol{r}}$-quantization axis,

$$\begin{aligned}
|+,+;\hat{\boldsymbol{r}}\rangle_{\rm out} &= |+,\hat{\boldsymbol{r}}\rangle_1|+,-\hat{\boldsymbol{r}}\rangle_2,\\
|+,-;\hat{\boldsymbol{r}}\rangle_{\rm out} &= |+,\hat{\boldsymbol{r}}\rangle_1|-,-\hat{\boldsymbol{r}}\rangle_2,\\
|-,+;\hat{\boldsymbol{r}}\rangle_{\rm out} &= |-,\hat{\boldsymbol{r}}\rangle_1|+,-\hat{\boldsymbol{r}}\rangle_2,\\
|-,-;\hat{\boldsymbol{r}}\rangle_{\rm out} &= |-,\hat{\boldsymbol{r}}\rangle_1|-,-\hat{\boldsymbol{r}}\rangle_2.
\end{aligned} \tag{14}$$

Unlike the incoming states (11), the spatial part for the scattered waves correspond to spherical outgoing waves with fixed parity under exchange of the two atoms, thus they are not included into the definitions of the outgoing scattering states here. The $\hat{\boldsymbol{r}}$-quantization is a must as the scattered particles move along the direction of $\boldsymbol{r}$, thus their helicities are defined with respect to the outgoing along the direction of $\boldsymbol{r}$. Among the four, $|+,+;\hat{\boldsymbol{r}}\rangle_{\rm out}$ and $|-,-;\hat{\boldsymbol{r}}\rangle_{\rm out}$ are antisymmetrized. The $|+,-;\hat{\boldsymbol{r}}\rangle_{\rm out}$ and $|-,+;\hat{\boldsymbol{r}}\rangle_{\rm out}$ do not have fixed exchange symmetry by themselves. They always appear together in antisymmetrized linear combinations.

For identical spin-1/2 fermions we study here, the subspace of $(F_t = \text{odd}, M_t)$ contains only two outgoing states $|+,-;\hat{\boldsymbol{r}}\rangle_{\rm out}$ and $|-,+;\hat{\boldsymbol{r}}\rangle_{\rm out}$. The subspace of $(F_t = \text{even} > 0, M_t)$ contains all four outgoing states, except for $F_t = 0$, where only two states are involved: $|+,+;\hat{\boldsymbol{r}}\rangle_{\rm out}$ and $|-,-;\hat{\boldsymbol{r}}\rangle_{\rm out}$. This point will become clearer after the spatial wave functions are explicitly substituted into the Schrodinger equation for two atoms.

In the ultracold regime, we affirm that the cross sections or the particle fluxes in higher-F_t spaces can be neglected, due to the same reason which gives rise to the ubiquitous Wigner threshold law for single channel scattering by a spherically symmetric short ranged potential at low energies. In the dominant $(F_t = 0, M_t = 0)$ subspace, the radial functions $G_\alpha^{F_t}(r)$ satisfy the two-by-two coupled-channel equations, which are given explicitly below,

$$\left[-\left(\frac{\hbar^2}{m}\frac{d^2}{dr^2} + E\right)\begin{pmatrix} 1 & 0\\ 0 & 1\end{pmatrix} + \widehat{V}_{F_t=0}\right]\begin{bmatrix} G_{F=0l=0}^{F_t=0}(r)\\ G_{F=1l=1}^{F_t=0}(r)\end{bmatrix} = 0, \tag{15}$$

where the effective potential in the $F_t = 0$ subspace is

$$\widehat{V}_{F_t=0} = \begin{bmatrix} V^{(0)}(r) & 2i\hbar^2 C_{\rm so}(\frac{d}{dr} + \frac{1}{r})/m\\ 2i\hbar^2 C_{\rm so}(\frac{d}{dr} - \frac{1}{r})/m & V^{(1)}(r) + 2\hbar^2/mr^2\end{bmatrix}. \tag{16}$$

This form of a coupled Schrödinger equation between different channels (radial functions) is a general feature of scattering with SOC. An earlier study used an ansatz for the scattering solution that forbids cross channel scattering, the results thus correspond to that of two single channels [24].

The SOC gives rise to the off-diagonal terms in Eq. (16), which cannot be neglected even at infinite interparticle separation. To properly include their effect on the scattering, the scattering K matrix is now determined through the correct asymptotic solutions as in the following

$$G^{F_t}/r\big|_{r\to\infty} \sim \mathcal{J}^{F_t} - \mathcal{Y}^{F_t} K^{F_t} \ , \tag{17}$$

where

$$\mathcal{J}^{F_t=0} = \begin{bmatrix} \frac{1}{\sqrt{2}}k_1 j_0(k_1 r) & -\frac{1}{\sqrt{2}}k_3 j_0(k_3 r)\\ -i\frac{1}{\sqrt{2}}k_1 j_1(k_1 r) & -i\frac{1}{\sqrt{2}}k_3 j_1(k_3 r)\end{bmatrix}, \tag{18}$$

and

$$\mathcal{Y}^{F_t=0} = \begin{bmatrix} \frac{1}{\sqrt{2}}k_1 y_0(k_1 r) & -\frac{1}{\sqrt{2}}k_3 y_0(k_3 r)\\ -i\frac{1}{\sqrt{2}}k_1 y_1(k_1 r) & -i\frac{1}{\sqrt{2}}k_3 y_1(k_3 r)\end{bmatrix}, \tag{19}$$

where $k_1 = \sqrt{k_{\rm so}^2 + k^2} - k_{\rm so}$ and $k_3 = \sqrt{k_{\rm so}^2 + k^2} + k_{\rm so}$, as illustrated in Fig. 2 are the corresponding low and high canonical momenta in the two helicity states $|+,+;\hat{\boldsymbol{r}}\rangle_{\rm out}$ and $|-,-;\hat{\boldsymbol{r}}\rangle_{\rm out}$. $j_l(x)$ and $y_l(x)$ are the spherical Bessel

functions [38]. The $\mathcal{J}^{F_t=0}$ and $\mathcal{Y}^{F_t=0}$ are the exact regular and irregular analytic solutions of Eq. (16) in the absence of any interaction potentials or for $V^{(0)} = V^{(1)} \equiv 0$. The two columns of the above matrices respectively correspond to solutions at k_1 and k_3. They are associated with the $|+,+;\hat{\boldsymbol{r}}\rangle_{\rm out}$ and $|-,-;\hat{\boldsymbol{r}}\rangle_{\rm out}$ states, which justifies our early statement that the helicity states $|+,-;\hat{\boldsymbol{r}}\rangle_{\rm out}$ and $|-,+;\hat{\boldsymbol{r}}\rangle_{\rm out}$ are not involved in the lowest total angular momentum subspace of $F_t = 0$ we consider. In this two-dimensional subspace, when no ambiguity arises, we also adopt a shorthand notation for the outgoing channels, using $|1\rangle_{\rm out}$ (for $|+,+;\hat{\boldsymbol{r}}\rangle_{\rm out}$) and $|3\rangle_{\rm out}$ (for $|-,-;\hat{\boldsymbol{r}}\rangle_{\rm out}$) to index the various matrix elements. For spin-$\frac{1}{2}$ fermions in the presence of an isotropic Rashba SOC, the low energy collision can then be most conveniently visualized as scattering from the two incoming states $|+,+;\boldsymbol{k}_1\rangle_{\rm in}$ and $|-,-;\boldsymbol{k}_3\rangle_{\rm in}$ into the two outgoing helicity state manifold of $|+,+;\hat{\boldsymbol{r}}\rangle_{\rm out}$ and $|-,-;\hat{\boldsymbol{r}}\rangle_{\rm out}$.

The above formulation for two spin-$\frac{1}{2}$ particles with SOC is very general, applicable for arbitrary energy (below the hyperfine splitting when applied to ^{6}Li) and SOC coupling strength. In reality, both experimental realizations of SOC [7–10] and the very validity of the Hamiltonian used to describe it, imply that we are most interested in a regime of SOC being weak, in the following sense. Let r_0 be the range of interaction without SOC, determined by equating the kinetic energy $(\hbar^2/2\mu)(1/r_0^2)$ to the van der Waals energy at r_0 [33]. The energy scale of SOC, s_E, is generally much smaller than the energy scale associated with the shorter-range van der Waals interaction. This criterion, which is equivalent to the length scale separation, $1/k_{\rm so} \gg r_0$, basically ensures that the SOC and other interactions are important in different regions and are not important simultaneously [29, 30]. Under such a condition, scattering in the presence of SOC can be solved in terms of scattering in the absence of SOC. Specifically, the K matrix, as defined by Eq. (17), can be obtained by matching Eq. (17), in a region of $r_0 \ll r \ll 1/k_{\rm so}$, to inner solutions for which the SOC is negligible. This is conceptually similar to the multiscale quantum-defect treatment of two atoms in a trap [30].

Other scattering matrices such as the S matrix can be defined in a similar manner with their usual relationships maintained. For example, the S matrix is related to the K matrix by $S^{F_t} = (I+iK^{F_t})(I-iK^{F_t})^{-1}$, where I is the identity matrix. The complete scattering information can then be extracted as in the standard scattering theory [39]. We note that in standard multichannel scattering theory without SOC (see, e.g., Ref. [37]), $\mathcal{J}^{F_t}$ and $\mathcal{Y}^{F_t}$ would have been diagonal.

After a rather lengthy calculation, we find analytically all linear independent solutions at large r for all total angular momentum subspaces $(F_t M_t)$. When properly matched to their corresponding short range solutions in the absence of SOC, the complete scattering solutions are found [39]. For the lowest total angular momentum subspace of $F_t = 0$, which gives dominant contributions at low energies, the scattered waves defining the S-matrix are given by the following

$$
\begin{aligned}
\Psi_{|+,+;\boldsymbol{k}_1\rangle_{\rm in}\to|+,+;\hat{\boldsymbol{r}}\rangle_{\rm out}}(\boldsymbol{r},\chi) &= \sqrt{2}\,\frac{e^{ik_1 r}}{r}\,\frac{S^{F_t=0}_{1,1}-1}{2ik_1}|+,+;\hat{\boldsymbol{r}}\rangle_{\rm out},\\
\Psi_{|+,+;\boldsymbol{k}_1\rangle_{\rm in}\to|-,-;\hat{\boldsymbol{r}}\rangle_{\rm out}}(\boldsymbol{r},\chi) &= \sqrt{2}\,\frac{e^{ik_3 r}}{r}\,\frac{S^{F_t=0}_{3,1}}{2ik_1}|-,-;\hat{\boldsymbol{r}}\rangle_{\rm out},\\
\Psi_{|-,-;\boldsymbol{k}_3\rangle_{\rm in}\to|+,+;\hat{\boldsymbol{r}}\rangle_{\rm out}}(\boldsymbol{r},\chi) &= \sqrt{2}\,\frac{e^{ik_1 r}}{r}\,\frac{S^{F_t=0}_{1,3}}{2ik_3}|+,+;\hat{\boldsymbol{r}}\rangle_{\rm out},\\
\Psi_{|-,-;\boldsymbol{k}_3\rangle_{\rm in}\to|-,-;\hat{\boldsymbol{r}}\rangle_{\rm out}}(\boldsymbol{r},\chi) &= \sqrt{2}\,\frac{e^{ik_3 r}}{r}\,\frac{S^{F_t=0}_{3,3}-1}{2ik_3}|-,-;\hat{\boldsymbol{r}}\rangle_{\rm out},
\end{aligned}
\tag{20}
$$

where the outgoing spherical waves are indicative of their being scattered and propagating radially outwards with the corresponding canonical momentum k_j. The first index i of the S-matrix element $S_{i,j}$ is the shorthand notation for the outgoing states $|i=1\rangle_{\rm out}$ and $|i=3\rangle_{\rm out}$ since the other two outgoing states are not involved in the $F_t = 0$ subspace, while the second index j is the shorthand notation for the incoming states $|i=1\rangle_{\rm in}$ and $|i=3\rangle_{\rm in}$ defined earlier in (11). This simplified index scheme within the $F_t = 0$ subspace will be adopted for all discussions in the following. The scattered particles give rise to outgoing fluxes which can be analogously calculated from the above scattering solutions (20), and we find

$$
\boldsymbol{j}^{F_t=0}_{|i\rangle_{\rm in}\to|j\rangle_{\rm out}}(\boldsymbol{r}) = \frac{\hbar}{m}\sqrt{k_{\rm so}^2+k^2}\,\frac{|S^{F_t=0}_{j,i}-\delta_{ij}|^2}{k_i^2}\,\frac{\hat{\boldsymbol{r}}}{r^2}, \tag{21}
$$

for $i,j \in \{1,3\}$. The various cross sections can be then defined properly in terms of the ratios of the scattered flux densities to the incoming particle flux densities, which then gives

$$
\sigma[\,|i\rangle_{\rm in}\to|j\rangle_{\rm out}] = \frac{2\pi}{k_i^2}\left|S^{F_t=0}_{j,i}-\delta_{ij}\right|^2. \tag{22}
$$

As we emphasized before, in the presence of SOC, the distinction between canonical and kinetic momentum is crucial for a proper definition of scattering cross sections in terms of particle flux densities.

IV. RESULTS AND DISCUSSIONS

In this section, we present the results from the lowest total angular momentum subspace of $F_t = 0$. Results for higher total angular momentum subspaces of $F_t > 0$ will be presented elsewhere as they do not provide meaningful contributions at low scattering energies [39].

For energies much greater than s_E, we obtain the K matrix to be given by the K matrix in the $\{F, l\}$ basis through a frame transformation. For $F_t = 0$, e.g., we obtain

$$K^{F_t=0} = U^{F_t=0\dagger} \begin{pmatrix} \tan\delta_{l=0}^{F=0} & 0 \\ 0 & \tan\delta_{l=1}^{F=1} \end{pmatrix} U^{F_t=0} , \quad (23)$$

where $U^{F_t=0}$ is a global unitary matrix

$$U^{F_t=0} = \frac{1}{\sqrt{2}} \begin{pmatrix} 1 & -1 \\ -i & -i \end{pmatrix} , \quad (24)$$

which transforms the diagonal K matrix in the absence of SOC in the spin singlet and triplet basis into the proper two dimensional helicity basis of shorthand notations 1 and 3 in the total $F_t = 0$ subspace. This result, together with similar results for other total angular momenta, has a very simple physical interpretation. It states that for energies much greater than the SOC energy scale, SOC has no effect on the scattering dynamics, except to facilitate the preparation and detection of particles in the helicity basis. This result is also confirmed by our analytical solutions Eqs. (17), (18), and (19). At higher energies, $k_1 \sim k_3 \sim k$, the matrix solutions Eqs. (18) and (19) indeed correspond to that obtained from solutions in the singlet and triplet basis in the absence of SOC transformed by the above frame transformation matrix (24). In the absence of SOC, the same K matrix describes scattering in the helicity basis, and is applicable for all (positive) energies.

For energies comparable or smaller than s_E, the length scale separation ensures that we are well into the region dominated by the s wave scattering, which is well characterized, for the vast majority of systems, by the universal behaviors of $\tan\delta_{l=0}^{F=0} \approx -a_{F=0}k$ and $\tan\delta_{l=1}^{F=1} \approx 0$. In this case, we obtain

$$K^{F_t=0} = -\frac{a_{F=0}}{k_1 + k_3} \begin{pmatrix} k_1^2 & -k_1 k_3 \\ -k_1 k_3 & k_3^2 \end{pmatrix} . \quad (25)$$

We also obtain this same result from the analytic solution of Eq. (16) for the pseudo potential model of $V^{(0)} = \frac{2\pi\hbar^2 a_{F=0}}{\mu}\delta(\boldsymbol{r})\frac{\partial}{\partial r}(r\cdot)$ and $V^{(1)} \equiv 0$ [40]. Technically, such an approach is equivalent to imposing the boundary conditions of $G^{F_t=0}_{F=0l=0}(r) \overset{r\to 0}{\sim} Ar(1 - a_{F=0}/r)$ and $G^{F_t=0}_{F=1l=1}(r) \overset{r\to 0}{\sim} 0$, consistent with the modified Bethe-Peierls boundary condition of Zhang *et. al.*, which gives $G^{F_t=0}_{F=1l=1}(r)/r \overset{r\to 0}{\sim} \text{const.} \propto k_{\rm so}$, beyond the divergent term v_p/r^2 in several recent studies on the same topic [25, 26, 41, 42]. For low energy collisions, terms proportional to the p-wave scattering volume v_p or higher are neglected as their contributions are vanishingly small. Our result, however, contains more information. For instance, it includes higher order terms relating to the s-wave effective range and the p-wave scattering volume without SOC, as well as scattering amplitudes in the higher F_t subspaces [39]. Both of the above two aspects will be reported elsewhere. In addition, unlike [25, 26], our result takes the form of simple analytical expressions. The multiscale QDT approach contains the pseudo potential results [30]. It is more general and leaves room for future generalizations, including both the cases of non-universal behavior around $a_{F=0} = 0$ [33] and the case of much stronger SOC, the treatment of the latter would be similar to the treatment of hyperfine effects in atomic scattering [29].

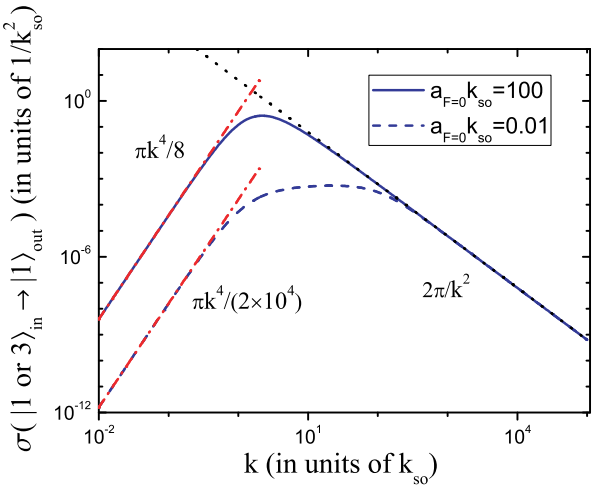

FIG. 3. (color online) The k-dependence of the cross sections $\sigma[\,|1\rangle_{\rm in} \to |1\rangle_{\rm out}]$ and $\sigma[\,|3\rangle_{\rm in} \to |1\rangle_{\rm out}]$ of Eq. (26). The limits of small k are discussed in the main text. The dotted line is the $\sim 1/k^2$ unitarity limit, while the dot-dashed lines denote the modified Wigner threshold limit of $\sim k^4$ at small k.

The K matrix of Eq. (25) immediately gives the following set of cross sections for ultracold collisions in the presence of SOC

$$\begin{aligned} &\sigma[\,|1\rangle_{\rm in} \to |1\rangle_{\rm out}] = \sigma[\,|3\rangle_{\rm in} \to |1\rangle_{\rm out}] \\ &= 8\pi a_{F=0}^2 \frac{k_1^2}{(k_3+k_1)^2 + a_{F=0}^2(k_3^2+k_1^2)^2} , \quad (26) \\ &\sigma[\,|1\rangle_{\rm in} \to |3\rangle_{\rm out}] = \sigma[\,|3\rangle_{\rm in} \to |3\rangle_{\rm out}] \\ &= 8\pi a_{F=0}^2 \frac{k_3^2}{(k_3+k_1)^2 + a_{F=0}^2(k_3^2+k_1^2)^2} . \quad (27) \end{aligned}$$

In comparison, the cross sections in the absence of SOC, determined by the K matrix of Eq. (23) in the helicity

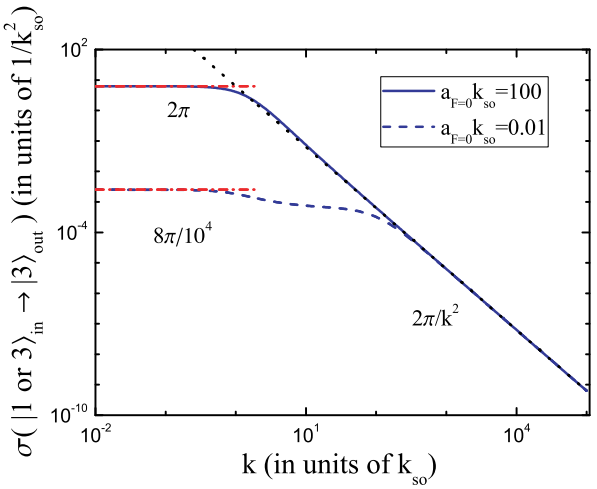

FIG. 4. (color online) The same as in Fig. 3 but for the scattering cross sections $\sigma[\,|1\rangle_{\rm in} \to |3\rangle_{\rm out}]$ and $\sigma[\,|3\rangle_{\rm in} \to |3\rangle_{\rm out}]$ of Eq. (27). The modified threshold limit becomes $\sim a_{F=0}^2$ and $\sim 1/k_{\rm so}^2$ respectively for $k_{\rm so}a_{F=0} \ll 1$ and $k_{\rm so}a_{F=0} \gg 1$.

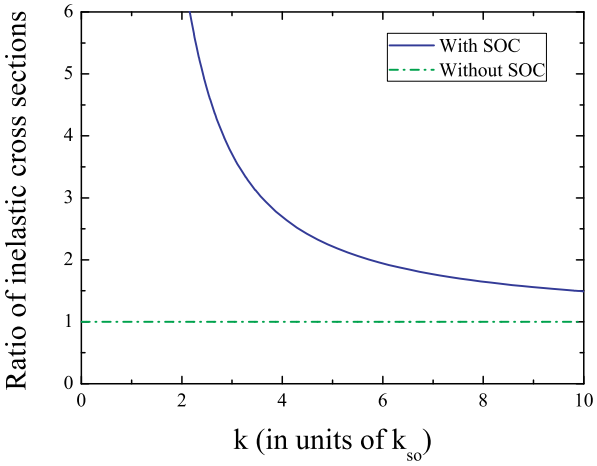

FIG. 5. (color online) The universal ratios of inelastic scattering cross sections, $\sigma[\,|1\rangle_{\rm in} \to |3\rangle_{\rm out}]/\sigma[\,|3\rangle_{\rm in} \to |1\rangle_{\rm out}]$, with (solid line) and without SOC (dash-dot line), as a function of k. The result with SOC is guaranteed by the time-reversal symmetry to be valid at all energies. The result without SOC is guaranteed by a combination of time-reversal and parity conservations to be valid at all energies. The difference is due to the break of parity conservation by SOC.

basis, are given in the s wave region by

$$\begin{aligned}&\sigma[\,|1\rangle_{\rm in} \to |1\rangle_{\rm out}] = \sigma[\,|3\rangle_{\rm in} \to |1\rangle_{\rm out}]\\ &= \sigma[\,|1\rangle_{\rm in} \to |3\rangle_{\rm out}] = \sigma[\,|3\rangle_{\rm in} \to |3\rangle_{\rm out}]\\ &= \frac{2\pi a_{F=0}^2}{1+a_{F=0}^2k^2}\,,\end{aligned} \tag{28}$$

which all follow the Wigner threshold behavior [31] of $\sigma \sim$ const. at small k.

Equations (26)-(28) are the main results of this work. They represent the universal behaviors satisfied by the vast majority of spin-$\frac{1}{2}$ systems in the ultracold regime. The strength of SOC only affects length and energy scaling. With proper rescaling, different systems differ from each other only in a single dimensionless parameter of $\eta_{\rm so} \equiv k_{\rm so}a_{F=0}$, with $\eta_{\rm so} = \infty$ corresponding to the unitarity limit.

In the high k end when $k > k_{\rm so}$ (still within the low energy collision limit), we see the characteristic $4\pi/k^2$ dependence in the presence of SOC. This is the same as the s-wave unitarity limit (28) when SOC is absent. It is reduced by a factor of two due to the use of helicity basis outgoing states.

The small k behavior of $k < k_{\rm so}$, however, show surprising new physics due to SOC. We focus here on two aspects of physics contained in these results. First, the SOC substantially modifies the threshold behavior, from the Wigner threshold law of $\sigma \sim$ const. for all cross sections, to

$$\sigma[\,|1\rangle_{\rm in} \to |1\rangle_{\rm out}] = \sigma[\,|3\rangle_{\rm in} \to |1\rangle_{\rm out}] \sim \frac{\pi a_{F=0}^2}{2k_{\rm so}^4}k^4, \tag{29}$$

$$\sigma[\,|1\rangle_{\rm in} \to |3\rangle_{\rm out}] = \sigma[\,|3\rangle_{\rm in} \to |3\rangle_{\rm out}] \sim 8\pi a_{F=0}^2, \tag{30}$$

for $k_{\rm so}a_{F=0} \ll 1$, and

$$\sigma[\,|1\rangle_{\rm in} \to |1\rangle_{\rm out}] = \sigma[\,|3\rangle_{\rm in} \to |1\rangle_{\rm out}] \sim \frac{\pi}{8k_{\rm so}^6}k^4, \tag{31}$$

$$\sigma[\,|1\rangle_{\rm in} \to |3\rangle_{\rm out}] = \sigma[\,|3\rangle_{\rm in} \to |3\rangle_{\rm out}] \sim \frac{2\pi}{k_{\rm so}^2}, \tag{32}$$

for $k_{\rm so}a_{F=0} \gg 1$. They imply that the interaction in $|1\rangle_{\rm in}$ is dominated by inelastic scattering into the $|3\rangle_{\rm out}$ channel, while the interaction in $|3\rangle_{\rm in}$ is dominated by elastic collision within the $|3\rangle_{\rm out}$ channel. Figures 3 and 4 show illustrative k-dependence of the above two cross sections at selected values of the singlet scattering length $a_{F=0}$.

Magnetic field tuned Feshbach resonance in atomic systems has enabled interesting investigation of the many-body physics in BCS to BEC crossover, particularly concerning the universality regime when the scattering length $a_{F=0}$ changes from $-\infty \to \infty$. Many theoretical studies address this topic when synthetic SOC is included. Our results above show, however, that such extensions maybe improper as the scattering amplitude is now limited by either $a_{F=0}$ or $1/k_{\rm so}$ (instead of $1/k$ for without SOC), whichever is smaller. The strength of SOC, $k_{\rm so}$, thus introduces a lower momentum cut off. In the presence of SOC, when $a_{F=0}$ is tuned across a Feshback resonance, the scattering amplitude no longer diverges. When SOC is absent, our result recovers the usual scattering amplitude.

Second, particles are preferentially scattered into the lower-energy helicity state, the "$-$" state when $C_{\rm so} > 0$, as reflected by $\sigma[\,|1\rangle_{\rm in} \to |3\rangle_{\rm out}]$ being always greater

than $\sigma[\,|3\rangle_{\rm in} \to |1\rangle_{\rm out}]$. More specifically

$$\frac{\sigma[\,|1\rangle_{\rm in} \to |3\rangle_{\rm out}]}{\sigma[\,|3\rangle_{\rm in} \to |1\rangle_{\rm out}]} = \frac{k_3^2}{k_1^2} = \left(\frac{\sqrt{1+(k/k_{\rm so})^2}+1}{\sqrt{1+(k/k_{\rm so})^2}-1}\right)^2 > 1\ ,$$

at all positive energies and diverges as $k_{\rm so}^4/k^4$ around the threshold. This result for the ratio of inelastic cross sections is applicable not only in the ultracold region, but at arbitrary energy as a result of the time-reversal symmetry [35]. To put it into perspective, we note that in the absence of SOC, the two inelastic cross sections are strictly equal at all energies as guaranteed by a combination of time-reversal and parity conservations. The two universal ratios are compared in Fig. 5. In an ultracold sample with SOC, the $|1\rangle_{\rm in}$ state has a finite cross section to be converted into $|3\rangle_{\rm out}$, and the $|3\rangle_{\rm in}$ state interacts mostly elastically, namely remains in the $|3\rangle_{\rm out}$, interactions in other states are negligible. Independent of initial statistical distribution, such a system has a single unique steady state to evolve into: one made of only particles in the lower-energy helicity state. We recall that the spin states of $|3\rangle_{\rm in}$ and $|3\rangle_{\rm out}$ as specified in Eqs. (11) and (14) respectively correspond to both atoms in their lower helicity states. In other words, a system of pure handedness develops spontaneously through interactions.

V. CONCLUSIONS

In conclusion, we have developed a general formalism for the scattering of two spin-$\frac{1}{2}$ particles in the presence of an isotropic SOC of the Rashba type. This represents a rigorous first attempt for a complete formulation of cold atom scattering in a non-Abelian gauge field. We have derived the universal analytic results in the ultracold regime and discussed their implications. Of particular importance is the modified scattering properties at low energies which shines new light on the active research into the many body physics of cold atoms with synthetic gauge fields. Many of the concepts introduced are generally applicable, and provide important guidance for investigations of other spin systems as well as anisotropic SOC. The theory developed here thus constitutes part of an essential foundation for understanding interacting many-body and few-body systems with SOC.

All of our results presented have been independently verified through analytic solutions for a square-well model potential [39]. The generality of our formulation and the incorporation of MQDT allow its easy generalization to virtually arbitrary energy including the energy region of $E < 0$. These topics will be addressed elsewhere.

ACKNOWLEDGMENTS

We thank Drs. Zhan Xu, Rong Lv, Xingcan Dai, Peng Zhang, and Zhifang Xu for helpful discussions. This work is supported by NSFC (No. 91121005 and No. 11004116), MOST 2013CB922000 of the National Key Basic Research Program of China, and the research program 2010THZO of the Tsinghua University.

[1] C. Chin, R. Grimm, P. Julienne, and E. Tiesinga, Rev. Mod. Phys. **82**, 1225 (2010).
[2] S. Giorgini, L. P. Pitaevskii, and S. Stringari, Rev. Mod. Phys. **80**, 1215 (2008).
[3] T. Kraemer, M. Mark, P. Waldburger, J. G. Danzl, C. Chin, B. Engeser, A. D. Lange, K. Pilch, A. Jaakkola, H.-C. Nägerl, and R. Grimm, Nature **440**, 315 (2006).
[4] E. Braaten and H.-W. Hammer, Physics Reports **428**, 259 (2006).
[5] C. H. Greene, Physics Today **63**, 40 (2010).
[6] J. Dalibard, F. Gerbier, G. Juzeliūnas, and P. Öhberg, Rev. Mod. Phys. **83**, 1523 (2011).
[7] Y.-J. Lin, K. Jiménez-García, and I. B. Spielman, Nature **471**, 83–6 (2011).
[8] P. Wang, Z.-Q. Yu, Z. Fu, J. Miao, L. Huang, S. Chai, H. Zhai, and J. Zhang, Phys. Rev. Lett. **109**, 095301 (2012).
[9] T.-L. Ho and S. Zhang, Phys. Rev. Lett. **107**, 150403 (2011).
[10] L. W. Cheuk, A. T. Sommer, Z. Hadzibabic, T. Yefsah, W. S. Bakr, and M. W. Zwierlein, Phys. Rev. Lett. **109**, 095302 (2012).
[11] M. Z. Hasan and C. L. Kane, Rev. Mod. Phys. **82**, 3045 (2010).
[12] X.-L. Qi and S.-C. Zhang, Rev. Mod. Phys. **83**, 1057 (2011).
[13] D. S. Novikov, Phys. Rev. B **76**, 245435 (2007).
[14] J. P. Vyasanakere and V. B. Shenoy, Phys. Rev. B **83**, 094515 (2011).
[15] Z. F. Xu, R. Lü, and L. You, Phys. Rev. A **83**, 053602 (2011).
[16] J. P. Vyasanakere, S. Zhang, and V. B. Shenoy, Phys. Rev. B **84**, 014512 (2011).
[17] M. Gong, S. Tewari, and C. Zhang, Phys. Rev. Lett. **107**, 195303 (2011).
[18] Z.-Q. Yu and H. Zhai, Phys. Rev. Lett. **107**, 195305 (2011).
[19] H. Hu, L. Jiang, X.-J. Liu, and H. Pu, Phys. Rev. Lett. **107**, 195304 (2011).
[20] Z. F. Xu and L. You, Phys. Rev. A **85**, 043605 (2012).
[21] B. M. Anderson, G. Juzeliūnas, V. M. Galitski, and I. B. Spielman, Phys. Rev. Lett. **108**, 235301 (2012).
[22] Z. F. Xu, Y. Kawaguchi, L. You, and M. Ueda, Phys. Rev. A **86**, 033628 (2012).
[23] J. P. Vyasanakere and V. B. Shenoy, New Journal of Physics **14**, 043041 (2012).
[24] X. Cui, Phys. Rev. A **85**, 022705 (2012).
[25] P. Zhang, L. Zhang, and Y. Deng, Phys. Rev. A **86**, 053608 (2012).
[26] P. Zhang, L. Zhang, and W. Zhang, Phys. Rev. A **86**,

042707 (2012).
[27] R. A. Williams, L. J. LeBlanc, K. Jimez-Garc, M. C. Beeler, A. R. Perry, W. D. Phillips, and I. B. Spielman, Science **335**, 314 (2012).
[28] B. Deb and L. You, Phys. Rev. A **64**, 022717 (2001).
[29] B. Gao, E. Tiesinga, C. J. Williams, and P. S. Julienne, Phys. Rev. A **72**, 042719 (2005).
[30] Y. Chen and B. Gao, Phys. Rev. A **75**, 053601 (2007).
[31] E. P. Wigner, Phys. Rev. **73**, 1002 (1948).
[32] J. R. Taylor, *Scattering Theory* (Wiley, New York, 1972).
[33] B. Gao, Phys. Rev. A **80**, 012702 (2009).
[34] B. Gao, Phys. Rev. A **84**, 022706 (2011).
[35] L. D. Landau and E. M. Lifshitz, *Quantum Mechanics* (Pergamon Press, Oxford, 1977).
[36] N. F. Mott and H. S. W. Massey, *The Theory of Atomic Collisions* (Oxford University Press, London, 1965).
[37] B. Gao, Phys. Rev. A **54**, 2022 (1996).
[38] F. W. J. Olver, D. W. Lozier, R. F. Boisvert, and C. W. Clark, eds., *NIST Handbook of Mathematical Functions* (NIST and Cambridge University Press, Cambridge, 2010).
[39] H. Duan, Ph.D. thesis, Tsinghua University, (to be published, 2013).
[40] K. Huang and C. N. Yang, Phys. Rev. **105**, 767 (1957).
[41] L. Zhang, J.-Y. Zhang, S.-C. Ji, Z.-D. Du, H. Zhai, Y. Deng, S. Chen, P. Zhang, and J.-W. Pan, Phys. Rev. A **87**, 011601(R) (2013).
[42] L. Zhang, Y. Deng, and P. Zhang, arXiv:1211.6919.